Article

Large-Scale Synthesis of Nearly Monodisperse CdSe/CdS Core/Shell Nanocrystals Using Air-Stable Reagents via Successive Ion Layer Adsorption and Reaction

J. Jack Li, Y. Andrew Wang, Wenzhuo Guo, Joel C. Keay, Tetsuya D. Mishima, Matthew B. Johnson, and Xiaogang Peng

J. Am. Chem. Soc., **2003**, 125 (41), 12567-12575• DOI: 10.1021/ja0363563 • Publication Date (Web): 23 September 2003

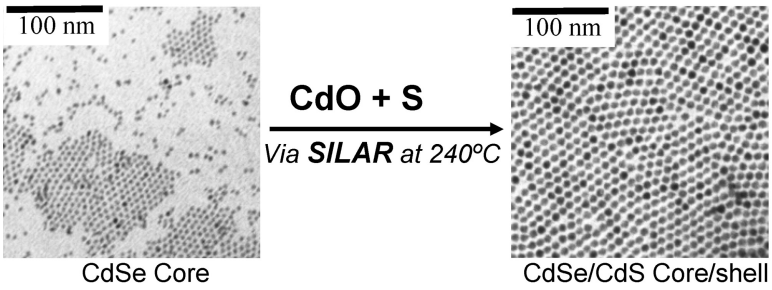

More About This Article

Additional resources and features associated with this article are available within the HTML version:

- Supporting Information
- Links to the 106 articles that cite this article, as of the time of this article download
- Access to high resolution figures
- Links to articles and content related to this article
- Copyright permission to reproduce figures and/or text from this article

View the Full Text HTML

J|A|C|S
ARTICLES
Published on Web 09/23/2003

Large-Scale Synthesis of Nearly Monodisperse CdSe/CdS Core/Shell Nanocrystals Using Air-Stable Reagents via Successive Ion Layer Adsorption and Reaction

J. Jack Li,[†] Y. Andrew Wang,[‡,§] Wenzhuo Guo,[†] Joel C. Keay,[‡,||] Tetsuya D. Mishima,[‡,||] Matthew B. Johnson,[‡,||] and Xiaogang Peng*[,†,‡]

Contribution from the Department of Chemistry & Biochemistry, University of Arkansas, Fayetteville, Arkansas 72701, Joint MRSEC at the University of Oklahoma and the University of Arkansas, Nanomaterials and Nanofabrication Laboratories (NN-Labs), Fayetteville, Arkansas 72703, and Department of Physics and Astronomy, University of Oklahoma, Norman, Oklahoma 73019

Received May 27, 2003; E-mail: xpeng@comp.uark.edu

Abstract: Successive ion layer adsorption and reaction (SILAR) originally developed for the deposition of thin films on solid substrates from solution baths is introduced as a technique for the growth of high-quality core/shell nanocrystals of compound semiconductors. The growth of the shell was designed to grow one monolayer at a time by alternating injections of air-stable and inexpensive cationic and anionic precursors into the reaction mixture with core nanocrystals. The principles of SILAR were demonstrated by the CdSe/CdS core/shell model system using its shell-thickness-dependent optical spectra as the probes with CdO and elemental S as the precursors. For this reaction system, a relatively high temperature, about 220−240 °C, was found to be essential for SILAR to fully occur. The synthesis can be readily performed on a multigram scale. The size distribution of the core/shell nanocrystals was maintained even after five monolayers of CdS shell (equivalent to about 10 times volume increase for a 3.5 nm CdSe nanocrystal) were grown onto the core nanocrystals. The epitaxial growth of the core/shell structures was verified by optical spectroscopy, TEM, XRD, and XPS. The photoluminescence quantum yield (PL QY) of the as-prepared CdSe/CdS core/shell nanocrystals ranged from 20% to 40%, and the PL full-width at half-maximum (fwhm) was maintained between 23 and 26 nm, even for those nanocrystals for which the UV−vis and PL peaks red-shifted by about 50 nm from that of the core nanocrystals. Several types of brightening phenomena were observed, some of which can further boost the PL QY of the core/shell nanocrystals. The CdSe/CdS core/shell nanocrystals were found to be superior in comparison to the highly luminescent CdSe plain core nanocrystals. The SILAR technique reported here can also be used for the growth of complex colloidal semiconductor nanostructures, such as quantum shells and colloidal quantum wells.

Introduction

Colloidal semiconductor nanocrystals are of great fundamental and industrial interest due to their size-dependent properties and flexible processing chemistry.[1−3] For many purposes, epitaxially grown core/shell semiconductor nanocrystals are of critical importance. If the shell possesses a higher band gap than the core material and the band offsets of the core/shell structures are type-I (the core possesses a lower conduction band and a higher valence band in comparison to those of the shell), a photogenerated electron and hole inside the nanocrystal will be mostly confined in the core. Consequently, such core/shell nanocrystals typically show bright photoluminescence (PL)[4−11] and electroluminescence[12−14] and are more stable against photo-oxidation.[5] For example, the PL quantum yield (QY) of core/shell nanocrystals can be as high as 50−80%,[4−6,11] although 10−40% PL QY is more routinely achieved.[12,15−18] Our most recent results reveal that core/shell nanocrystals may also be

[†] University of Arkansas.
[‡] Joint MRSEC.
[§] Nanomaterials and Nanofabrication Laboratories.
[||] University of Oklahoma.

(1) Brus, L. *J. Phys. Chem.* **1986**, *90*, 2555−60.
(2) Alivisatos, A. P. *Science* **1996**, *271*, 933−937.
(3) Heath, J. R., Ed. *Special Issue for Nanostructures*, 1999.
(4) Hines, M. A.; Guyot-Sionnest, P. *J. Phys. Chem.* **1996**, *100*, 468−470.
(5) Peng, X.; Schlamp, M. C.; Kadavanich, A. V.; Alivisatos, A. P. *J. Am. Chem. Soc.* **1997**, *119*, 7019−7029.
(6) Dabbousi, B. O.; RodriguezViejo, J.; Mikulec, F. V.; Heine, J. R.; Mattoussi, H.; Ober, R.; Jensen, K. F.; Bawendi, M. G. *J. Phys. Chem. B* **1997**, *101*, 9463−9475.
(7) Micic, O. I.; Smith, B. B.; Nozik, A. J. *J. Phys. Chem. B* **2000**, *104*, 12149−12156.
(8) Cao, Y.; Banin, U. *J. Am. Chem. Soc.* **2000**, *122*, 9692−9702.
(9) Manna, L.; Scher, E. C.; Li, L.-S.; Alivisatos, A. P. *J. Am. Chem. Soc.* **2002**, *124*, 7136−7145.
(10) Cumberland, S. L.; Hanif, K. M.; Javier, A.; Khitrov, G. A.; Strouse, G. F.; Woessner, S. M.; Yun, C. S. *Chem. Mater.* **2002**, *14*, 1576−1584.
(11) Reiss, P.; Bleuse, J.; Pron, A. *Nano Lett.* **2002**, *2*, 781−784.
(12) Schlamp, M. C.; Peng, X. G.; Alivisatos, A. P. *J. Appl. Phys.* **1997**, *82*, 5837−5842.
(13) Mattoussi, H.; Radzilowski, L. H.; Dabbousi, B. O.; Thomas, E. L.; Bawendi, M. G.; Rubner, M. F. *J. Appl. Phys.* **1998**, *83*, 7965−7974.
(14) Tesster, N.; Medvedev, V.; Kazes, M.; Kan, S.; Banin, U. *Science* **2002**, *295*, 1506−1508.
(15) Bruchez, M.; Moronne, M.; Gin, P.; Weiss, S.; Alivisatos, A. P. *Science* **1998**, *281*, 2013−2016.

more chemically and thermally stable than the corresponding plain core nanocrystals.[19] Recent advancement in the synthesis of semiconductor nanocrystals has made it possible to obtain highly luminescent plain core nanocrystals.[20−23] Unfortunately, the stability and processibility of plain core nanocrystals are both far from ideal, and for many reasons this instability and poor processibility may be intrinsic.[19,22] Therefore, core/shell nanocrystals are the desired structures when either the nanocrystals must undergo complicated chemical treatments, such as for biomedical applications,[15,16,24,25] or the nanocrystals require constant excitation as for LEDs[12−14] and lasers.[26]

The quality of core/shell nanocrystals[4−6,9−11,27−30] has not yet reached that of plain core nanocrystals in terms of size and size distribution control. Two critical issues for maintaining the size distribution of nanocrystals during the growth of shell materials include: (1) the elimination of the homogeneous nucleation of the shell materials; and (2) homogeneous monolayer growth of shell precursors onto all core nanocrystals in solution, yielding shell layers with nearly the same thickness around each core nanocrystal. In principle, the reactivity of the precursors should be weak enough to prevent independent nucleation, but sufficiently strong to promote the epitaxial growth around the existing core nanocrystals. Therefore, the relatively stable, inexpensive, and relatively safe alternative precursors[31] should be more suited for the growth of high-quality core/shell nanocrystals than the traditional organometallic precursors, such as dimethyl cadmium, dimethyl zinc, and trismethylsilane sulfide.

Less active precursors are much easier to control as has been demonstrated in the case of the development of the alternative synthetic schemes for high-quality plain core nanocrystals.[22,32−36] A brief report on the synthesis of CdSe/ZnSe core/shell nanocrystals using zinc stearate as the zinc precursor and Se-trioctylphosphine as the Se precursor in a coordinating solvent by Reiss et al. was published recently.[11] Unfortunately, not much structural characterization was reported, although an impressively high PL efficiency was demonstrated. Based on the limited information, it is clear that the size distribution of the core/shell nanocrystals was significantly worse than that of the original core nanocrystals, although Reiss et al. were very careful in choosing the growth conditions (dropwise addition of the shell growth solution). This fact and our own preliminary results have convinced us that alternative precursors alone are unlikely to be sufficient for the improvement of the size distribution of the core/shell nanocrystals.

A very interesting concept, atomic-layer-epitaxy (ALE), in the molecular beam expitaxy (MBE) literature[37] attracted our attention. In ALE, the molecular beams of the anionic and cationic species are switched on and off in an alternating pattern. In this way, only one-half of a monolayer will grow in each period with either the cationic or the anionic beam on. Because the cationic and anionic species do not coexist with each other in the growth chamber, local nucleation on the substrate or in the gas phase is avoided. Consequently, the thin film grows in a well-controlled manner. This concept was extended to the deposition of thin films onto solid substrates using solution bath, successive ion layer adsorption and reaction (SILAR).[38,39] The impressive results recently demonstrated by Park et al.[39] revealed that SILAR is a very successful technique for the growth of high-quality thin films.

In this work, we apply the SILAR concept toward the growth of core/shell nanocrystals in solution. To test the principle and optimize the growth conditions, we chose CdSe/CdS core/shell nanocrystals as our model system. The shell-thickness-dependent optical properties of this system provide a convenient probe to determine the size and size distribution of the resulting nanocrystals during growth.

Experimental Section

Materials. Cadmium oxide (99.99%), selenium (99.5%, 100 mesh), sulfur (99.98%, powder), trioctylphosphine oxide (TOPO, 90%), tributylphosphine (TBP, 97%), 1-octadecene (ODE), oleic acid (OA, 90%), and octadecylamine (ODA, 97%) were purchased from Aldrich. Stearic acid (99%) was obtained from Avocado. All organic solvents were purchased from EM Sciences. All chemicals were used directly without any further purification.

Choice of Reaction System. Octadecene **(**ODE) was selected as the only noncoordinating solvent for both core nanocrystals and the two injection solutions. Its relatively low melting point (below 20 °C), relatively high boiling point (about 320 °C), low cost, low toxicity, low reactivity to precursors, and excellent solvation power for many compounds at elevated temperatures make ODE an ideal solvent for the growth of high-quality nanocrystals in general.[35,36] CdO and elemental sulfur were chosen as the precursors for the growth of the CdS shell onto the CdSe core nanocrystals. Octyldecylamine (ODA) was used as the ligands for the core/shell nanocrystals because alkylamines have proven to be good ligands for highly luminescent plain CdSe core[21,22] and CdSe/CdS core/shell nanocrystals.[5]

Synthesis of CdSe Core Nanocrystals. Highly fluorescent CdSe nanocrystals were made by a procedure modified from those reported previously.[22,35] For a typical reaction, the mixture of 0.2 mmol of CdO, 0.8 mmol of stearic acid, and 2 g of ODE in a 25 mL three-neck flask was heated to about 200 °C to obtain a colorless clear solution. After this solution was cooled to room temperature, ODA (1.5 g) and 0.5 g

(16) Mattoussi, H.; Mauro, J. M.; Goldman, E. R.; Anderson, G. P.; Sundar, V. C.; Mikulec, F. V.; Bawendi, M. G. *J. Am. Chem. Soc.* **2000**, *122*, 12142−12150.
(17) Sundar, V. C.; Lee, J.; Heine, J. R.; Bawendi, M. G.; Jensen, K. F. *Adv. Mater.* **2000**, *12*, 1102−1104.
(18) Coe, S.; Woo, W.-K.; Bawendi, M.; Bulovic, V. *Nature* **2002**, *420*, 800−803.
(19) Guo, W.; Li, J. J.; Wang, Y. A.; Peng, X. *J. Am. Chem. Soc.* **2003**, *125*, 3901−3909.
(20) Hines, M. A.; Guyot-Sionnest, P. *J. Phys. Chem. B* **1998**, *102*, 3655−3657.
(21) Talapin, D.; Rogach, A. L.; Kornowski, A.; Haase, M.; Weller, H. *Nano Lett.* **2001**, *1*, 207.
(22) Qu, L.; Peng, X. *J. Am. Chem. Soc.* **2002**, *124*, 2049−2055.
(23) de Donega, C.; Hickey, S. G.; Wuister, S. F.; Vanmaekelbergh, D.; Meijerink, A. *J. Phys. Chem. B* **2003**, *107*, 489−496.
(24) Chan, W. C. W.; Nie, S. M. *Science* **1998**, *281*, 2016−2018.
(25) Han, M.; Gao, X.; Su, J. Z.; Nie, S. *Nat. Biotechnol.* **2001**, *19*, 631−635.
(26) Klimov, V. I.; Mikhailovsky, A. A.; Xu, S.; Malko, A.; Hollingsworth, J. A.; Leatherdale, C. A.; Eisler, H. J.; Bawendi, M. G. *Science* **2000**, *290*, 314−317.
(27) Kortan, A. R.; Hull, R.; Opila, R. L.; Bawendi, M. G.; Steigerwald, M. L.; Carroll, P. J.; Brus, L. E. *J. Am. Chem. Soc.* **1990**, *112*, 1327−1332.
(28) Hoener, C. F.; Allan, K. A.; Bard, A. J.; Campion, A.; Fox, M. A.; Mallouk, T. E.; Webber, S. E.; White, J. M. *J. Phys. Chem.* **1992**, *96*, 3812−3817.
(29) Mews, A.; Eychmueller, A.; Giersig, M.; Schooss, D.; Weller, H. *J. Phys. Chem.* **1994**, *98*, 934−941.
(30) Tian, Y.; Newton, T.; Kotov, N. A.; Guldi, D. M.; Fendler, J. H. *J. Phys. Chem.* **1996**, *100*, 8927−8939.
(31) Qu, L.; Peng, Z. A.; Peng, X. *Nano Lett.* **2001**, *1*, 333−336.
(32) Peng, Z. A.; Peng, X. *J. Am. Chem. Soc.* **2001**, *123*, 183−184.
(33) Peng, Z. A.; Peng, X. *J. Am. Chem. Soc.* **2002**, *124*, 3343−3353.
(34) Peng, X. *Chem.-Eur. J.* **2002**, *8*, 334−339.
(35) Yu, W. W.; Peng, X. *Angew. Chem., Int. Ed.* **2002**, *41*, 2368−2371.
(36) Battaglia, D.; Peng, X. *Nano Lett.* **2002**, *2*, 1027−1030.
(37) Herman, M. A.; Sitter, H. *Molecular Beam Epitaxy: Fundamentals and Current Status*, 2nd rev. and updated ed.; Springer: New York, 1996.
(38) Ristov, M.; Sinadinovski, G.; Grozdanov, I.; Mitreski, M. *Thin Solid Films* **1989**, *173*, 53−8.
(39) Park, S.; Clark, B. L.; Keszler, D. A.; Bender, J. P.; Wager, J. F.; Reynolds, T. A.; Herman, G. S. *Science* **2002**, *297*, 65.

of TOPO were added into the flask. Under argon flow, this system was reheated to 280 °C. At this temperature, a selenium solution made by dissolving 2 mmol of Se in 0.472 g of TBP and further diluting with 1.37 g of ODE was quickly injected. The growth temperature was then reduced to 250 °C. Typically this reaction generates CdSe nanocrystals of about 3.5 nm in size with the first absorption peak around 570 nm. The reaction mixture was allowed to cool to room temperature, and an extraction procedure[40] was used to purify the nanocrystals from side products and unreacted precursors. The nanocrystals remained in the hexanes/ODE layer, and the unreacted precursors and excess amines were extracted into the methanol layer. The particle concentration of the purified CdSe solution in hexanes, as stock solution for core/shell growth, was measured using Beer's law with the reported extinction coefficients of CdSe nanocrystals.[40] The TOPO-coated CdSe nanocrystals were synthesized using the procedure described previously.[41]

Two loading methods were tested for the CdSe core nanocrystals. In the first method, the nanocrystals were never precipitated out of solution; they were directly loaded as a solution in hexanes. The purification of the core nanocrystals was performed by an extraction method developed recently.[35,40] The second loading method was similar to the one reported in the literature for the growth of CdSe/CdS nanocrystals,[5] for which the core nanocrystals were purified by precipitation/decantation and the precipitate was loaded into the reaction flask. Experimental results revealed that the first approach, the solution-based loading, was necessary for the growth of high-quality core/shell nanocrystals. TEM measurements verified that aggregates/fused particles were formed by precipitation of the amine-coated CdSe nanocrystals. All of the results discussed below were obtained using the solution-based loading.

Injection Solutions. The cadmium injection solution (0.04 M) was prepared by dissolving CdO (0.615 g) in oleic acid (10.83 g) and ODE (108 mL) at 250 °C. The sulfur injection solution (0.04 M) was prepared by dissolving sulfur in ODE at 200 °C. Both injection solutions were made under an Ar flow. After clear solutions were obtained, the Cd injection solution was allowed to cool to about 60 °C and the sulfur injection solution was allowed to cool to room temperature. For each injection, a calculated amount of a given injection solution was taken with a syringe using a standard air-free procedure.

Calculations for the Injections. The SILAR technique is based on the alternating injections of the Cd and S precursors into the solution containing CdSe nanocrystals for the growth of CdSe/CdS core/shell nanocrystals. The amount of cadmium or sulfur precursors required for each layer was determined by the number of the surface atoms of a given size of a core/shell nanocrystal. Because there is only about 5−6% lattice mismatch between CdSe and CdS bulk crystals, the calculations were based on the wurtzite structure of CdSe nanocrystals. The average thickness of one monolayer of CdS was taken as 0.35 nm, so one additional layer growth would increase the diameter of a nanocrystal by 0.7 nm. For example, in a typical experiment with 1×10^{-5} mmol of 3.7 nm core, 2.13×10^{-3} mmol of Cd and S precursors is needed for the first layer of the shell growth, and an additional 2.85×10^{-3} mmol of Cd and S precursors completes the growth of the second layer.

A Typical SILAR Synthesis. CdSe nanocrystals (3.5 nm in diameter, 1.01×10^{-4} mmol of particles) dissolved in 2.44 g of hexanes were mixed with 1.5 g of ODA and 5.0 g of ODE in a 25 mL three-neck flask. The flask was then pumped down at room temperature with a mechanical pump for 30 min to remove the hexanes and at 100 °C for another 5−10 min to remove any residual air from the system. Subsequently, the system was switched to Ar flow and the reaction mixture was further heated to 240 °C for the injections. The first injection was 0.49 mL of the Cd injection solution (0.04 M), and the amounts of the subsequent injection solutions were calculated using the method described above. To monitor the reaction, aliquots were taken at the first minute after each injection and every 3−5 min after that for absorption measurements. If there was no observable change in the UV−vis absorption spectra for two successive aliquots, the injection of another shell component for either the same layer (*n*S) or the next layer ((*n* + 1)Cd) was executed. The reaction was terminated by allowing the reaction mixture to cool. The final product was diluted by hexanes followed by a methanol extraction, or the nanocrystals were precipitated by adding acetone into the hexanes solution. Excess amines were further removed by dissolving the nanocrystals in chloroform and precipitating them with acetone.

The reaction temperature was varied between 120 and 260 °C to study the temperature effect for the growth of CdSe/CdS core/shell nanocrystals. For these experiments, the other reaction conditions and procedures were kept the same as the typical synthesis.

Multigram-Scale Synthesis of CdSe/CdS Core/Shell Nanocrystals. The SILAR procedure was readily extended to a multigram scale. In a typical large-scale synthesis, 195 g of a hexanes solution containing CdSe nanocrystals (3.5 nm in size, 5.87×10^{-3} mmol of particles) was mixed with 250 g of ODE and 75 g of ODA in a three-neck flask. After removal of hexanes and air under vacuum, the mixture was heated to 240 °C in argon atmosphere for the injection and growth. Using the same injection solutions as were used in the small-scale synthesis, the amounts of the injection solutions injected for each step were as follows: 27 mL of the Cd and S solutions for the first layer, 37 mL of each injection solution for the second layer, 48.6 mL of each injection solution for the third layer, 61.8 mL of each injection solution for the fourth layer, and 76.6 mL of each injection solution for the fifth layer. With fast stirring in place, the injection solutions did not need to be added in a dropwise manner. The injection rate was only limited by the pore size of the needle, less than 1 s for an injection with 5 mL of solution. After the reaction, the raw products were separated by acetone precipitation followed by centrifugation. After purification, the argon-flow dried nanocrystals weighed about 2.5 g.

Optical Measurements. Absorption spectra were measured on an HP 8453 diode array spectrophotometer. Photoluminescence (PL) and photoluminescence excitation (PLE) were measured using a HITACHI F-2500 fluorescence spectrophotometer. PL quantum yield (QY) of the samples was determined using organic dyes with known quantum yield as the standard, following a previously reported method.[5,9,22] The PL QY data reported in this work were obtained using R640 as the standard, which gave us significantly lower values in comparison to those using LD690 as the reference.

Transmission Electron Microscopy (TEM). The low-resolution TEM images were taken on a JEOL 100CX transmission electron microscope with an acceleration voltage of 80 kV. All of the samples were purified by acetone precipitation from chloroform solution or hexanes/methanol extraction. Formvar film-coated copper grids were dipped in the hexanes or toluene solutions to deposit nanocrystals onto the film. Randomly oriented nanocrystals on the TEM substrate were obtained by using a diluted nanocrystal solution, with an absorbance of the first absorption peak of the nanocrystals below about 0.05. If the absorbance was above 0.2, densely packed monolayers and multilayers of nanocrystals were observed. Selected area electron diffraction patterns (SAED) were taken with a camera length of 120 cm.

High-resolution TEM pictures were taken using a JEOL 2000 FX microscope. The nanocrystals were deposited onto ultrathin carbon film, copper grids.

X-ray powder diffraction (XRD) patterns were obtained using a Philips PW1830 X-ray diffractometer. It was essential to remove excess ODA ligands to obtain meaningful diffraction patterns.

X-ray photoelectron spectroscopy (XPS) was performed under ultrahigh vacuum using Mg Kα radiation from a Fison/VG dual anode X-ray source with a VG100AX hemispherical analyzer. A 20 eV pass

(40) Yu, W. W.; Qu, L.; Guo, W.; Peng, X. *Chem. Mater.* **2003**, *15*, 2854−2860.
(41) Aldana, J.; Wang, Y.; Peng, X. *J. Am. Chem. Soc.* **2001**, *123*, 8844−8850.

energy was used for the elemental scans. All nanocrystals with different shell thicknesses, including the plain core nanocrystals, were taken from the same reaction and purified in a glovebox to remove unreacted precursors. The nanocrystals were dispersed in toluene and then pipetted onto a clean gold surface (Au/Cr/Si wafer). The toluene was allowed to evaporate before introduction into the vacuum.

The relative intensity variation of emitted electrons from the S, Se, and Cd atoms in the core/shell system was modeled using a simple Monte Carlo simulation. This simulation used a core diameter of 3.5 nm and a monolayer shell thickness of 0.35 nm. In this simulation, core-level photoelectrons associated with the appropriate chemical species were uniformly generated in the core (Se_{3p}, Cd_{3d}) and or shell (S_{2p}, Cd_{3d}). The total signal for each photoelectron core level was a weighted sum of the generated electrons. The generated electron were weighted by $\exp(-z\lambda)$, where z is the electron perpendicular path length out of the nanocrystal and λ is the electron inelastic mean free path (IMFP). The IMFP used was 21 Å for S_{2p} and Se_{3p} electrons and 17 Å for the Cd_{3d} 3d core electrons in CdSe and CdS, as determined from ref 42.

Photooxidation. The photooxidation experiments were performed using a standard method reported previously[41,43]or using the 514 nm line of an argon ion laser with 50−100 mW of power.[9] For the laser experiments, the beam diameter on the sample was 0.8 cm. Nanocrystals in oxygen or Ar were compared under the same conditions. Photoluminescence spectra were measured before and after radiation.

Thin Film Deposition. Plain core nanocrystals or core/shell nanocrystals were deposited onto glass or ITO substrates by spin coating from toluene solutions. The PL spectra of the thin films were taken by placing the substrates at the cross-point of the excitation beam and the normal direction of the detector, with a 30° angle relative to the excitation beam. The PL spectra of the two original solutions with the same absorbance at the excitation wavelength were compared. The PL spectra of the two thin film samples, CdSe nanocrystals and CdSe/CdS core/shell nanocrystals, were compared by normalizing PL intensity using the absorbance of thin films at the excitation wavelength.

The surface modification with mercaptopropionic acid for both core and core/shell nanocrystals was performed using the standard procedure reported previously.[41] The UV−vis and PL measurements were carried out using the purified nanocrystals dissolved in water.

Results

Reaction temperature played a critical role for the growth of CdS shell onto CdSe nanocrystals through SILAR in ODE. Figure 1 (top plot) illustrates the evolution of the UV−vis peak position of the core/shell nanocrystals after each injection of either cadmium or sulfur solution at different reaction temperatures. This evolution represents the effect of the shell thickness because for each run an identical core sample was used. Evidently, the accumulated thickness of the shell after each injection decreased systematically as the reaction temperature decreased. Temperature impact on the Cd injections was significantly stronger than that for the sulfur injections (Figure 1, top plot). This indicates that SILAR works best at high temperatures for this system.

Importantly, the absorption spectrum of the core nanocrystals in this reaction system did not show any noticeable change when the system was heated at 240 °C for at least 30 min without any injection, if the system was carefully degassed. The PL QY of the core nanocrystals increased in the first 5−15 min[21] and often decreased after the initial heating period at 240 °C. Even higher temperatures, for example, 260 °C and above, made it difficult to prevent Ostwald ripening of the core and core/shell nanocrystals. Except where explicitly indicated, all results in this report were obtained with the reaction temperature of 240 °C.

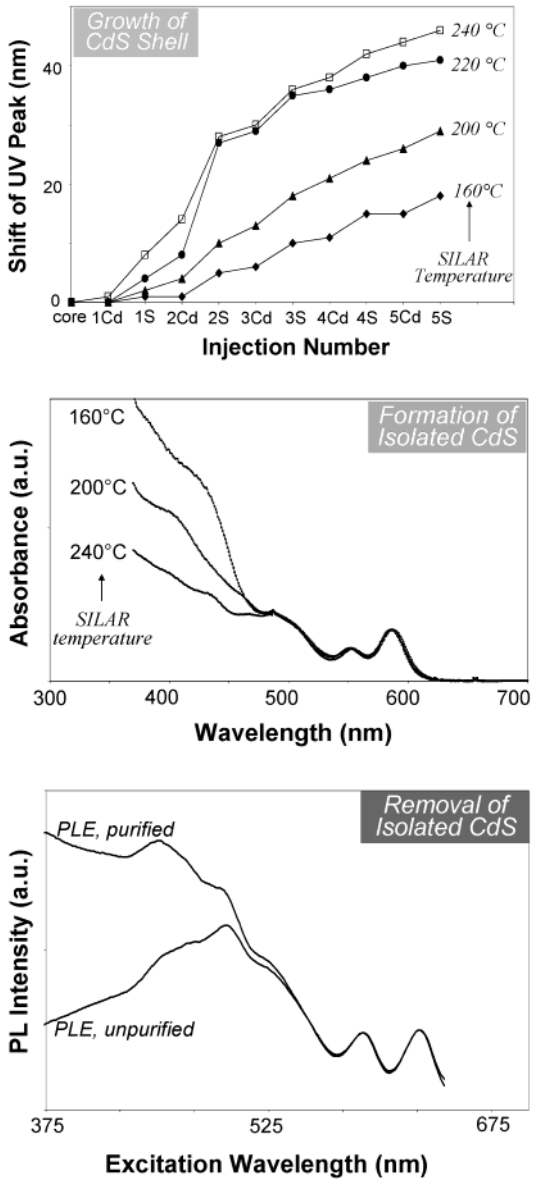

Figure 1. Top: The accumulative value of the red-shift of the first absorption peak for nanocrystals due to the growth of CdS shell after each injection plotted for different reaction temperatures. Middle: Formation of isolated CdS nanocrystals at relatively low temperatures, as evidenced by the extremely high, low wavelength absorbance even with a thin CdS shell. Bottom: PLE spectra (monitored at 650 nm) of CdSe/CdS nanocrystals before and after the removal of isolated CdS particles.

At lower temperatures, the Cd and S precursors added into the solution through injections did not grow on the surface of the existing nanocrystals; instead they formed isolated CdS nanocrystals through a homogeneous nucleation process. Figure 1 (middle plot) illustrates a spectral comparison of the CdSe/CdS core/shell nanocrystals with the same shell thickness grown on the same batch of core nanocrystals under different temperatures. Relative to the absorbance at the first absorption peak, the absorbance in the wavelength range below 500 nm for the

(42) Jablonski, C. J. P. a. A. *NIST Electron Inelastic-Mean-Free-Path Database-Version 1.1*; National Institute of Standards and Technology: Gaithersburg, MD, 2000.
(43) Wang, Y. A.; Li, J. J.; Chen, H.; Peng, X. *J. Am. Chem. Soc.* **2002**, *124*, 2293−2298.

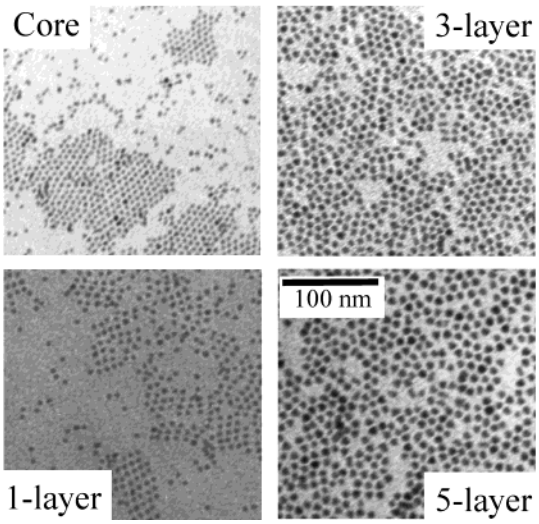

Figure 2. TEM images of CdSe plain core nanocrystals and the corresponding core/shell nanocrystals with different shell thickness from the same SILAR reaction.

low-temperature reactions increased rapidly, indicating the formation of individual CdS nanocrystals. It should be pointed out that, even at 240 °C, the formation of individual CdS nanocrystals may still occur when the shell thickness was more than four monolayers. This is probably due to inaccuracies in the amount of precursors added caused by calculation or experimental errors. For example, the growth of five monolayers of CdS shell onto CdSe nanocrystals with a size of 3.5 nm means that the total number of CdS units per particle is about 10 times greater than the original CdSe units. Therefore, a small initial error may result in significant inaccuracies for the thickest shells.

Fortunately, the isolated CdS nanocrystals formed in the growth process could easily be separated from the CdSe/CdS core/shell nanocrystals by extraction or precipitation. In the extraction method, CdS nanocrystals were extracted into the methanol layer from the hexanes/ODE layer containing CdSe/CdS core/shell nanocrystals. Under UV radiation, the methanol layer emitted blue light, and the hexanes/ODE layer exhibited the PL of the core/shell nanocrystals. After purification, the PLE spectra of the core/shell nanocrystals were dramatically different (Figure 1, bottom plot). As shown in Figure 1 (bottom plot), the existence of isolated CdS particles in the solution typically resulted in a significant drop of the PLE signal below 500 nm, due to the absorption of isolated CdS nanocrystals in that spectral window.

Size, shape, and size/shape distribution of the CdSe/CdS core/shell nanocrystals were controlled well using SILAR. Figure 2 shows four TEM images of CdSe plain core nanocrystals and the corresponding core/shell nanocrystals with different shell thicknesses. The increase of the TEM observed particle size correlates well with the numbers of CdS monolayers estimated from the injections. The nearly monodispersed core nanocrystals formed good, well-ordered two-dimensional (2D) superlattices. Similarily, core/shells with one or two monolayers of CdS shell formed well-ordered 2D superlattices. Core/shell nanocrystals with three or more monolayers of CdS formed superlattices with local order only. For such thick shells, the shape of the particles is noticeably elongated, and 2D superlattices do not form when the nanocrystals are randomly oriented. This occurs when the nanocrystals are deposited at low particle concentrations. Orientation of the elongated core/shell nanocrystals was achieved when they were deposited from a relatively concentrated solution (details in Experimental Section). For these conditions, it was possible to obtain superlattice packing with thousands of nanocrystals (Figure 3).

The appearance of almost all nanocrystals in the superlattice shown in Figure 3 is dot-shaped. This indicates that the nanocrystals themselves were oriented with their long axis perpendicular to the grid. The selected area electron diffraction (SAED) patterns, shown in Figure 3, further reveal that the *c*-axis of the nanocrystals in the superlattice was perpendicular to the substrate. Furthermore, the SAED pattern reveals that the long axis of the core/shell nanocrystals is the *c*-axis of the wurtzite structure. This result was further verified by high-resolution TEM measurements. As shown in Figure 4A and B, the shape of some of the five-layer nanocrystals was significantly elongated along the *c*-axis, close to a petal-shape. The dimension along the *c*-axis of the top two nanocrystals in Figure 4 is about 9 nm, and the dimension perpendicular to the *c*-axis is about 7 nm. A small portion of the core/shell nanocrystals with five-

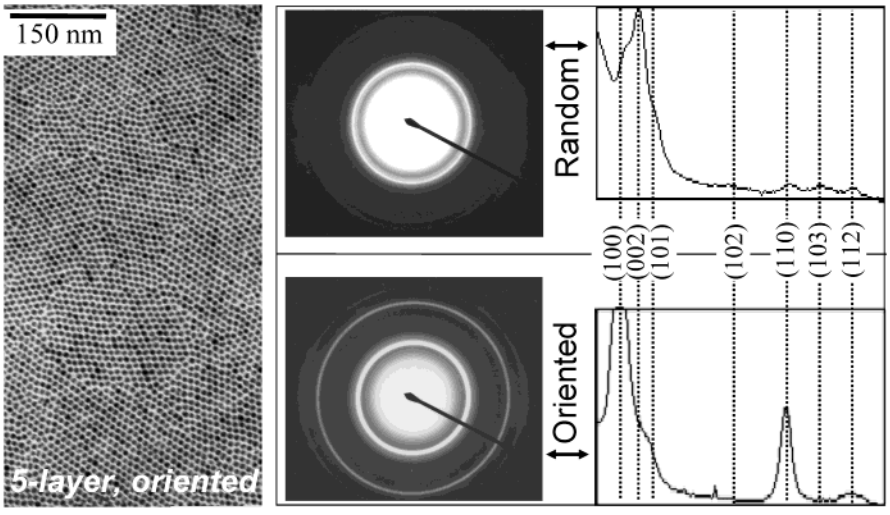

Figure 3. Core/shell nanocrystals with a thick five-monolayer CdS shell formed a superlattice only if the particle concentration of the deposition solution was high (left). The SAED patterns and the corresponding diffraction intensity profiles of randomly deposited (top row) and oriented (bottom row) core/shell nanocrystals.

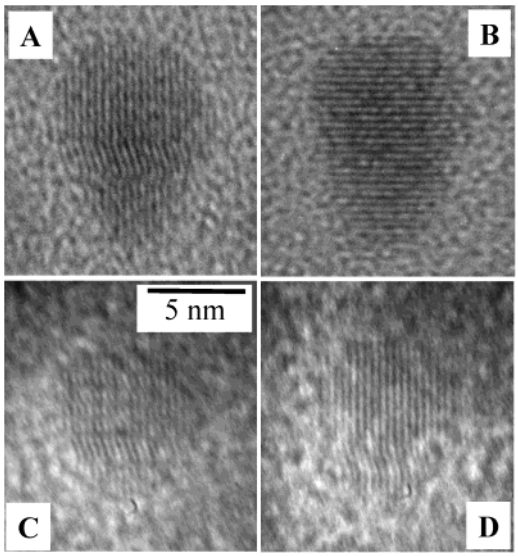

Figure 4. HRTEM images of four representative core/shell nanocrystals, 3.5 nm core with five monolayers of CdS shell.

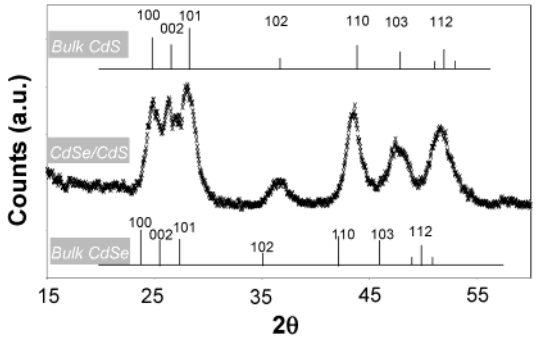

Figure 5. XRD pattern of core/shell nanocrystals, 3.5 nm core with five monolayers of CdS shell. For comparison, the standard powder diffraction patterns of wurtzite CdSe and CdS bulk crystals are provided.

layer CdS were found to be more close to a dot-shape (see bottom two images in Figure 4). Overall, the distribution of the aspect ratio of the core/shell nanocrystals with thick shells was not as narrow as that of the dimension of the short axis. Such elongation along the *c*-axis was also observed for plain core CdSe nanocrystals.[44] The existence of the elongation along the *c*-axis of the core/shell nanocrystals may either be caused by the elongation of the original core nanocrystals or indicate that growth of thick core/shell nanocrystals for this system might occur beyond a single monolayer at a time, possibly due to the inaccuracy in the addition of the monomers as mentioned above.

The X-ray diffraction patterns of the core/shell nanocrystals shifted from a wurtzite CdSe-like to a wurtzite CdS-like pattern upon an increase of the shell thickness. The same trend was observed previously,[5] although the previous report was only for CdSe/CdS core/shell nanocrystals with less than three monolayers of CdS shell. For the core/shell nanocrystals with a five-monolayer CdS shell, the diffraction pattern was almost the same as the CdS nanocrystals of the same size (Figure 5). The crystal domain size calculated using the Scherrer equation with the (110) peak is about 7 nm, which is consistent with the TEM results discussed above. The domination of the CdS pattern for the thick shell nanocrystals is expected given that the CdS:CdSe

(44) Murray, C. B.; Norris, D. J.; Bawendi, M. G. *J. Am. Chem. Soc.* **1993**, *115*, 8706−8715.

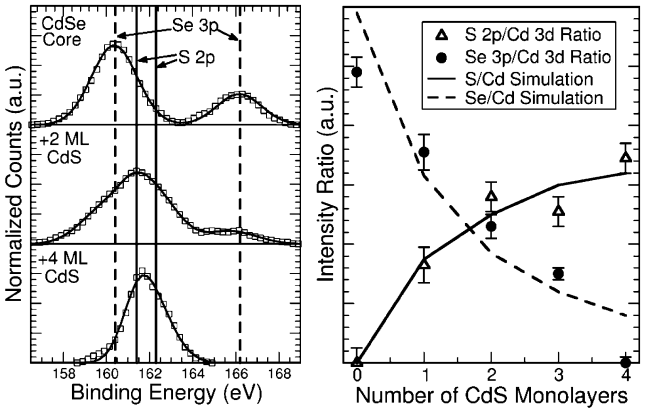

Figure 6. Left: XPS spectra of CdSe core and CdSe/CdS core/shell nanocrystals. Right: Comparison between experimental and simulation results of the S/Cd and Se/Cd ratio obtained by XPS measurements.

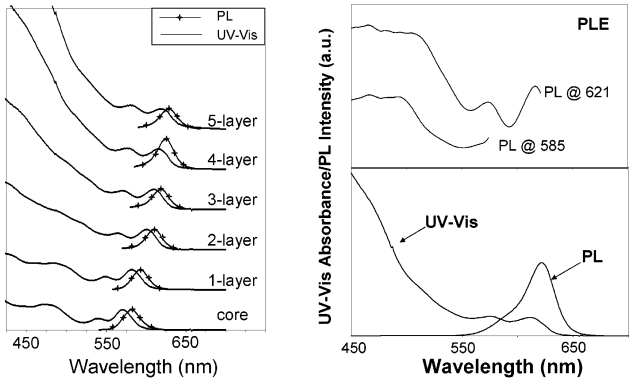

Figure 7. Left: The evolution of the UV−vis and PL spectra of the core/shell nanocrystals upon the growth of the CdS shell in a typical reaction. Right: Asymmetric PL of core/shell nanocrystals with five monolayers of CdS shell.

ratio is 10:1 for these nanocrystals. The relatively low peak height and large peak width of the (103) peak in comparison to the (110) peak in the diffraction pattern shown in Figure 5 are consistent with stacking faults perpendicular to the *c*-axis as observed by HRTEM (Figure 4).[44]

XPS measurements were performed for the CdSe/CdS core/shell nanocrystals.[5,28] As shown in Figure 6 (left panel), the Se_{3p} peaks decrease and the S_{2p} peaks increase as the shell thickness increased from zero to four monolayers. This directly indicates a uniform coating of the CdSe with the CdS shells. This uniformity of the shell growth is further confirmed by plotting the S and Se-to-Cd ratios versus the expected shell thickness (Figure 6, right). The comparison of these data to the computer simulation (solid and dashed lines) shows good agreement.

The UV−vis and PL spectra of the core/shell nanocrystals of a typical reaction are illustrated in Figure 7 (left panel). The sharp features of the absorption spectra and the narrow PL peaks are consistent with the narrow size distribution of the core/shell nanocrystals shown in Figures 2 and 3.

The PL spectrum of core/shell nanocrystals with thick shells typically had a shoulder on the high energy side, and the relative intensity of this shoulder increased by purifying away the side products and initial reactants (see more details below). Although the shoulder was about 35 nm blue-shifted from the band edge emission, the PLE features of the shoulder emission were only about 10 nm blue-shifted in comparison to those of the band

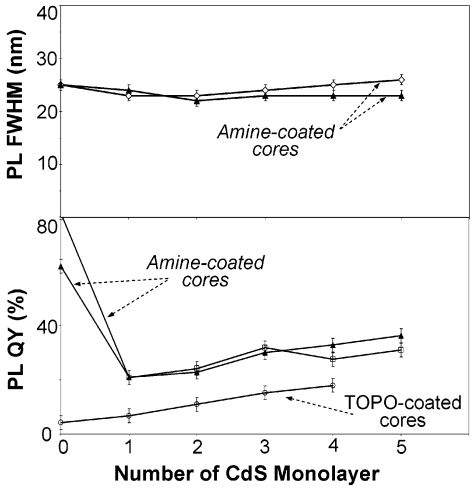

Figure 8. PL QY and PL fwhm of the as-prepared CdSe/CdS core/shell nanocrystals versus the number of CdS monolayers.

edge PLE (Figure 7, right panel). This indicates that the shoulder is not likely caused by a bimodal size distribution. The nature of this shoulder needs to be further studied. Possibly, this shoulder could be related to the spatially indirect PL[5] because the electron and hole wave functions of the exciton in CdSe/CdS core/shell nanocrystals with a thick CdS shell will be mostly localized in the shell and core materials, respectively.

PL QY and PL Full-Width at Half-Maximum (fwhm) of the Core/Shell Nanocrystals. Within the shell thickness explored in this work, the PL QY of the core/shell nanocrystals increased as the shell thickness increased (Figure 8). We observed that the PL QY of the plain core nanocrystals prior to the shell growth varied significantly even if the reactions were carried out with the same batch of the core nanocrystals as shown in Figure 8. However, with the same batch of cores, the peak positions, the PL QY, and the PL fwhm of the core/shell nanocrystals generated by two parallel reactions were similar (Figure 8).

Growth reactions with TOPO-coated cores generated core/shell nanocrystals with significantly lower PL QY in comparison to those with amine-coated cores, although a systematic increase of the PL QY was also observed for the increase of the shell thickness (Figure 8).

The PL fwhm of the core/shell nanocrystals maintained the original value of the original cores within the experimental error (Figure 8, top). This is consistent with good control of the size distribution of the core/shell nanocrystals mentioned above. However, the PL spectra of the core/shell nanocrystals with thick shells, five or more monolayers, often possessed a tail on the high energy side as discussed above.

Multigram-scale growth of core/shell nanocrystals was performed by using the SILAR method discussed above. The quality of the resulting nanocrystals was similar to that of the small scale synthesis. In fact, the TEM images shown in Figures 2 and 3 were all recorded with the nanocrystals generated by a large-scale synthesis that yielded about 2.5 g of core/shell nanocrystals. It was found that, even for this large-scale synthesis, dropwise addition of the precursor solutions was not necessary.

Darkening and brightening phenomena observed in this work are summarized in Figure 9. In the growth process, especially for those reactions that occurred at relatively low

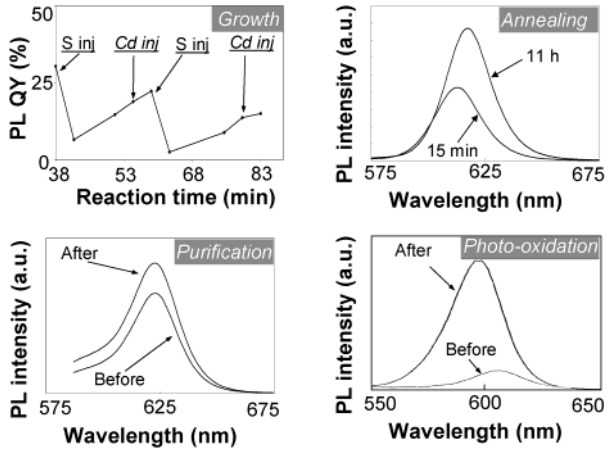

Figure 9. PL darkening and brightening phenomena observed in the growth and manipulation of CdSe/CdS core/shell nanocrystals.

temperatures, a darkening process was observed right after each injection of the sulfur stock solution. When this darkening was observed, a rapid increase of the shell thickness, indicated by a quick red-shift of the absorption peak, was always observed.

It has been previously reported for CdSe/ZnSe core/shell nanocrystals that the PL QY increased significantly by annealing the system at 190 °C for 1−1.5 h after the addition of all of the stock solution.[11] In the case of CdSe/CdS core/shell nanocrystals, annealing sometimes improved the PL QY. This was accompanied by a small red-shift of the emission peak (Figure 9). However, this brightening phenomenon was not found to be reproducible.

An unexpected brightening phenomenon was observed when the nanocrystals were purified using either the extraction or the precipitation method. The PL QY of the core/shell nanocrystals increased with the removal of the side products and unreacted precursors (Figure 9), although the emission peak retained the same position after purification. At this moment, it is not clear what type(s) of impurities in the solution affected the PL properties of the nanocrystals.

Manna et al. reported that laser-induced photoannealing brightened the PL of CdSe/CdS/ZnS core/shell rod-shaped nanocrystals.[9] The CdSe/CdS core/shell nanocrystals described in this work could also be brightened by photoradiation when oxygen was present in the solution. A brightening was always accompanied by a noticeable blue-shift of the absorption/PL spectrum, indicating that the size of the semiconductor nanocrystals decreased. These results imply that the photoinduced brightening phenomenon observed here is due to the photooxidation of the shell material. Interestingly, the rate of photooxidation of the core/shell nanocrystals was strongly dependent on the environment, although it occurred at a much slower rate in comparison to that for the corresponding plain core nanocrystals. In water or polar solvents, photooxidation of hydrophilic thiol-coated CdSe/CdS core/shell nanocrystals occurred at a relatively fast rate[19] (see the example shown in Figure 9). In nonpolar solvents, the oxidation of the ODA-coated core/shell nanocrystals required hours to days to show a noticeable change. When the core/shell nanocrystals were embedded in thin polymer films, no photooxidation was observed in air even with intense laser radiation for 1−2 h. Under the same conditions, the highly luminescent CdSe core nanocrystals were oxidized within minutes.[45]

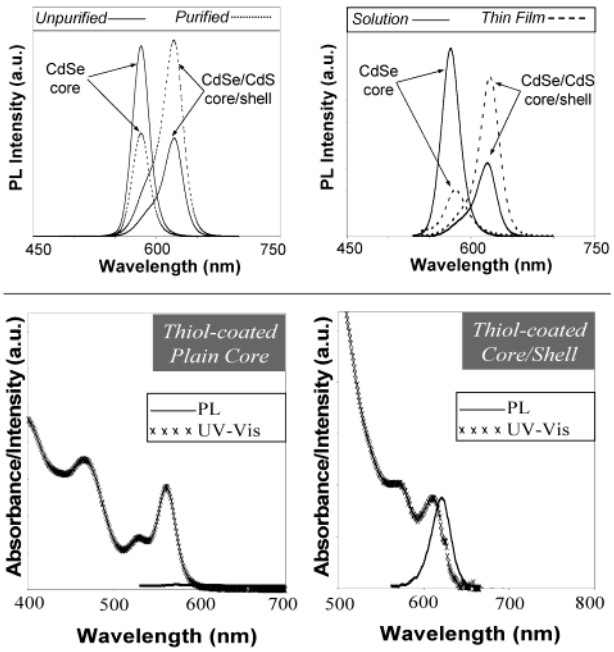

Figure 10. Comparison of the processibility of plain core and core/shell nanocrystals. Top-right: PL spectra of plain core and core/shell nanocrystals before and after purification by the precipitation/decantation procedure. Top-left: PL spectra of the plain core and core/shell nanocrystals upon the deposition of the nanocrystals onto substrates. Bottom: UV−vis and PL spectra of plain core and core/shell nanocrystals coated with hydrophilic thiols.

The processibility of the core/shell nanocrystals is superior to that of the corresponding core nanocrystals (Figure 10). As mentioned above, the PL QY of the core/shell nanocrystals increased after precipitation or extraction purification procedures, while the highly luminescent CdSe core nanocrystals' emission was almost extinguished after a parallel precipitation procedure. To maintain a reasonable PL brightness with the CdSe core nanocrystals, the purification must stop while a significant amount of free amine remains in the solution along with the plain core nanocrystals.

The free amine in the solution actually caused a serious problem when the plain core nanocrystals were deposited as thin films for devices, such as LEDs and lasers. The films were opaque with noticeable amounts of white impurities. Even with these free amines, the emission efficiency of the plain core nanocrystals dropped significantly after they were deposited as thin films. In contrast, the purified core/shell nanocrystals formed optically clear thin films using the same procedures. Furthermore, even though the core/shell nanocrystals in solution were less bright than the plain core nanocrystals dissolved in the same solvent, they appeared brighter in the form of solid films (Figure 10) due to a better preserved PL QY and less scattering.

A typical method to make hydrophobic semiconductor nanocrystals water soluble for purposes such as biomedical applications[15,16,24] is to replace the original hydrophobic ligands by hydrophilic thiols. After the amine ligands were replaced by hydrophilic thiols, the highly emitting plain core nanocrystals showed no emission (Figure 10). In contrast, the PL of the core/shell nanocrystals partially remained after the same treatment. Furthermore, the PL brightness of the thiol-coated core/shell CdSe/CdS nanocrystals can be partially recovered by controlled photochemical (Figure 9) or chemical oxidation.[19] Generally, the same oxidation treatments rapidly decomposed the plain core CdSe nanocrystals without any noticeable PL recovery.

Colloidal nanocrystals are often required to withstand harsh chemical and thermal treatments for certain applications. Our results revealed that the CdSe/CdS core/shell nanocrystals synthesized by SILAR are significantly more stable than the corresponding plain core nanocrystals under harsh processing conditions.[19]

Discussion

The epitaxial grown core/shell structure of the resulting nanocrystals can be determined using the criteria established previously. The immediate and significant red-shift of the absorption spectra after growth of each monolayer of CdS (Figures 1 and 7) indicated that the resulting nanocrystals are core/shell structures, rather than alloy structures.[5] XPS measurements directly confirmed a uniform layer-by-layer growth of the CdS shell (Figure 6).[5,28] The TEM and XRD measurements (Figures 4 and 5) indicate that the core/shell nanocrystals are single crystals. The lattice fringes including the stacking faults (Figure 4) for each nanocrystal extend completely across each nanocrystal, directly indicating epitaxial growth.[5]

The reaction temperature dramatically affects the growth of CdSe/CdS core/shell nanocrystals (Figure 1). The SILAR technique was only fully realized when the reaction temperature was sufficiently high. Evidently, the reactivity of the Cd precursor was the limiting factor. Interestingly, the competitive process, the formation of isolated CdS nanocrystals through homogeneous nucleation in solution, increased significantly at the lower reaction temperature (Figure 1). The general assumption that high temperatures should benefit homogeneous nucleation rather than epitaxial growth does not appear to be correct in the CdSe/CdS system. This abnormal phenomenon is an important feature of the layer-by-layer growth inherent in SILAR. At high temperatures, the Cd precursors were largely consumed by epitaxial growth prior to the addition of the S precursors, while for the S precursors, next added to the system, the only possibility was to grow onto the core/shell nanocrystals. In contrast, at low temperatures, the Cd precursors accumulated in the solution because of the energy barrier for epitaxial growth. After the subsequent introduction of the S precursors into the reaction solution, the accumulated Cd precursors react with the S to form isolated CdS nanocrystals. If a more reactive Cd precursor was employed, the temperature for epitaxial growth may be lowered. Systematic molecular level mechanistic studies should be helpful for the development of such Cd precursors with optimal reactivity.

PL properties of highly crystalline semiconductor nanocrystals are strongly dependent on the surface of the nanocrystals. For example, nanocrystals emit well only if ligands of a specific type are attached to the surface[46] and those ligands are coated on the surface under appropriate conditions, such as temperature[21,22] and photoradiation.[45] Similarly, the PL QY of the plain core nanocrystals dropped significantly after the growth of the first monolayer of the CdS shell because the relatively small band offsets between CdSe and CdS leave the CdSe/CdS core/

(45) Nazzal, A. Y.; Qu, L.; Peng, X.; Xiao, M. *Nano Lett.* **2003**, *3*, in press.

(46) Kuno, M.; Lee, J. K.; Dabbousi, B. O.; Mikulec, F. V.; Bawendi, M. G. *J. Chem. Phys.* **1997**, *106*, 9869−9882.

shell nanocrystals sensitive to environmental changes (Figure 9). The previous results revealed that amines are ideal ligands for the formation of highly emitting CdSe nanocrystals.[22,47,48] However, fatty acids are better ligands for CdS nanocrystals.[35,36] Unfortunately, SILAR growth of CdSe/CdS core/shell nanocrystals using fatty acids as the ligands at desired temperature was found to be difficult, which often resulted in precipitation of the nanocrystals. The different stability of amine-coated and carboxylate-coated CdSe/CdS core/shell nanocrystals may come from the net negative charges of the carboxylate groups. When the surface of a nanocrystal was switching between positive and negative charged states in a SILAR process, a neutral ligand should be beneficial.

The darkening phenomenon observed right after the introduction of the S precursors can be explained by the accompanied rapid growth of the core/shell nanocrystals because rapid growth causes disorder on the surface of nanocrystals.[22,47] Conversely, subsequent ordering may explain the brightening observed by annealing.

The results shown in Figure 10 and the related text in the Results section indicate that ODA ligands are bound tightly on the surface of the CdSe/CdS core/shell nanocrystals reported here. However, this is not the case for the corresponding CdSe core nanocrystals[22] or the CdSe/CdS core/shell nanocrystals synthesized at low temperatures.[5] The difference between the CdSe/CdS core/shell nanocrystals synthesized at different temperatures implies that higher temperatures promote the surface passivation with ODA ligands, through either a strong bonding or a high surface coverage. Further experiments are needed to distinguish these two possibilities.

The SILAR technique reported here has been proven to be versatile for the growth of complex semiconductor nanostructures in solution. Colloidal two-dimensional (2D) semiconductor nanostructures have been considered as a challenging task in the field of colloidal semiconductor nanocrystals. The intrinsic feature of the SILAR technique, a precise thickness control without homogeneous nucleation of the shell materials, has made it possible to grow high-quality colloidal quantum shells and colloidal quantum wells.[48]

Acknowledgment. Financial support from the NSF is acknowledged. J.J.L. is grateful for the Research Assistant Fellowship provided by the Center for Sensing Technology and Research (C-STAR) at the University of Arkansas.

JA0363563

(47) Talapin, D. V.; Rogach, A. L.; Shevchenko, E. V.; Kornowski, A.; Haase, M.; Weller, H. *J. Am. Chem. Soc.* **2002**, *124*, 5782−5790.
(48) Battaglia, D.; Li, J. J.; Wang, Y.; Peng, X. *Angew. Chem.* **2003**, accepted for publication.